

Thermodynamic Recycling in Quantum Computing: Demonstration Using the Harrow–Hassidim–Lloyd Algorithm and Information Erasure

Nobumasa Ishida* and Yoshihiko Hasegawa†

Department of Information and Communication Engineering,
Graduate School of Information Science and Technology,
The University of Tokyo, Tokyo 113-8656, Japan

Branch selection, including postselection, is a standard method for implementing nonunitary transformations in quantum algorithms. Conventionally, states associated with unsuccessful branches are discarded and treated as useless. Here we propose a generic framework that reuses these failure branches as thermodynamic resources. The central element is an athermal bath that is naturally generated during the reset of a failure branch. By coupling this bath to a target system prior to relaxation, useful thermodynamic tasks can be performed, enabling performance beyond conventional thermodynamic limits. As an application, we analyze information erasure and derive the resulting gain analytically. We further demonstrate the framework by implementing the Harrow–Hassidim–Lloyd algorithm on IBM’s superconducting quantum processor. Despite substantial noise and errors in current hardware, our method achieves erasure with heat dissipation below the Landauer limit. These results establish a practical connection between quantum computing and quantum thermodynamics and suggest a route toward reducing thermodynamic costs in future large-scale quantum computers.

Introduction—In quantum algorithms, branch selection based on measurement outcomes, including postselection, is widely used to implement nonunitary transformations of quantum states. As an example, the Harrow–Hassidim–Lloyd (HHL) algorithm [1] selects the branch that yields the desired solution state via an ancilla measurement. Furthermore, quantum singular-value transformation [2, 3], which unifies the HHL algorithms and other representative algorithms, realizes general transformations through measurement-based selection. In fault-tolerant quantum computing, magic-state distillation [4–6], an essential building block, also accepts the output only when the outcomes of multiple observable measurements are consistent. A common feature of these examples is that, among the branches generated during computation, the unsuccessful branches are discarded as meaningless states: these states must be reset to enable retries. Methods such as amplitude amplification and magic-state cultivation have been proposed to mitigate this issue [7–9], but none can completely avoid discarding qubits. Given the high cost of quantum computation, how to handle failure branches is relevant from the viewpoint of efficient use of computational resources.

In this work, we propose *thermodynamic recycling* as a framework that reuses failure branches in quantum algorithms by connecting them to a subsequent thermodynamic task, whose relevance in quantum computing has been recently highlighted [10–16]. The key component is an athermal bath that can arise as a byproduct during the reset of failure branches: in a reset using a cold bath, the bath can be driven into a nonequilibrium state while the failure branch is returned to its initial state. In our approach, we couple this athermal bath with a thermodynamic target system before it relaxes and perform the task operation (Fig. 1). This can enable

performance beyond the thermodynamic limits by using garbage states as resources. Thermodynamic recycling is a generic framework that does not rely on a specific algorithm or thermodynamic task.

We analyze information erasure as a representative example of a thermodynamic task. Information erasure reduces the entropy of a principal system and entails heat dissipation to a bath. Although heat dissipation in quantum computers should be minimized for their accurate operation [17, 18] especially in the context of quantum error correction [13, 14, 19], it is fundamentally unavoidable due to Landauer’s principle. However, by exploiting the athermal bath originating from failure branches via thermodynamic recycling, the heat dissipation can be reduced below this bound. We theoretically derive the gain responsible for such an improvement and analyze how the structure of branch selection affects the gain.

We demonstrate thermodynamic recycling on IBM’s superconducting quantum processor [20] by using the HHL algorithm, a practical algorithm with a postselection structure. Using a classical feedforward operation, we supply the failure branch state to the subsequent information-erasure task only when the algorithm fails, thereby preparing an athermal bath. Device noise and delays in the feedforward operation degrade the athermality of the bath. Nevertheless, our experimental results show a regime in which heat dissipation is reduced below the Landauer limit. This indicates that thermodynamic recycling is feasible under the constraints of current quantum computers. Our work strengthens the connection between quantum computing and thermodynamics and provides a guideline for reducing thermodynamic costs in future quantum computers.

Settings—We consider a computational system C consisting of qubits, and a finite-size bath B used for cooling

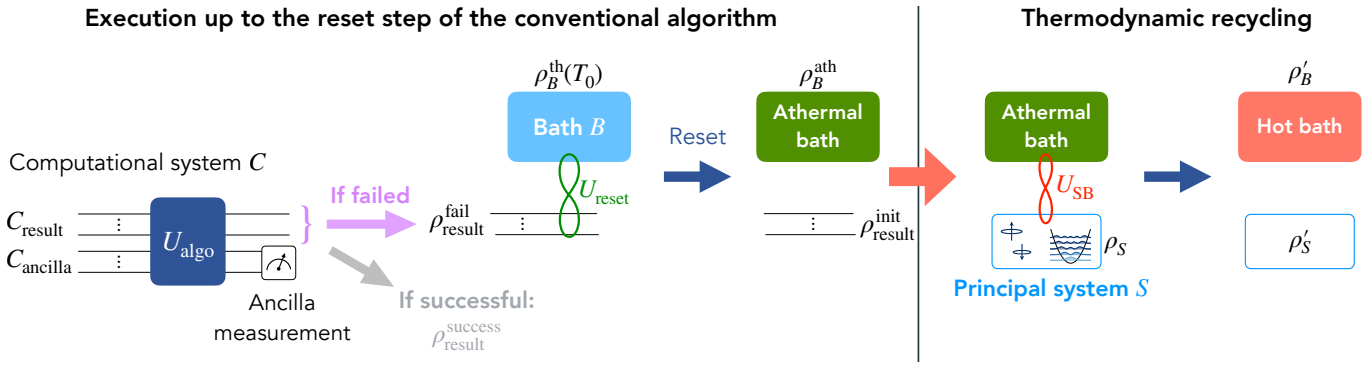


FIG. 1. Illustration of thermodynamic recycling. During the reset of a failure branch state after running an algorithm, the bath B can transition to an athermal state ρ_B^{ath} . Before relaxation, we couple it to the target system S and perform a thermodynamic task (information erasure in this work).

C . The bath is initially in the equilibrium state at a low temperature T_0 , $\rho_B^{\text{th}}(T_0) = 1/Z e^{-\beta H_B}$. Here H_B is the bath Hamiltonian, $\beta = 1/(k_B T_0)$ is the inverse temperature, k_B is the Boltzmann constant, and $Z = \text{Tr}[e^{-\beta H_B}]$ is the partition function. The qubits in C are initially cooled by the bath to the ground state $\rho_C = |0\dots0\rangle\langle0\dots0|$ approximately. We consider running an algorithm on C that includes branch selection. The overall process is shown in Fig. 1. After a unitary operation U_{algo} , we measure an ancilla subsystem of C and select the success/failure branch based on the outcome. We denote the non-ancilla part of C by C_{result} , i.e., $C = C_{\text{result}} + C_{\text{ancilla}}$. In the success branch, the state of C_{result} , $\rho_{\text{result}}^{\text{success}}$, gives the desired output state. In the failure branch, the state becomes an irrelevant state $\rho_{\text{result}}^{\text{fail}}$ and must be reset for a retry. In the standard operation of quantum computing, reset procedures include measurement-based resets and resets based on interaction with a bath [20–24]. Here, we focus on the latter from a thermodynamic viewpoint. That is, by the coupling unitary dynamics U_{reset} between C_{result} and the bath B ,

$$\rho_{\text{result}}^{\text{fail}} \otimes \rho_B^{\text{th}}(T_0) \xrightarrow{U_{\text{reset}}} \rho_{\text{result}}^{\text{init}} \otimes \rho_B^{\text{ath}}. \quad (1)$$

Here we assume that, after the reset, C_{result} is returned to the initial state for the next run, $\rho_{\text{result}}^{\text{init}} \approx |0\dots0\rangle\langle0\dots0|$, and is decoupled from the bath. In this process, the bath generally transitions to an athermal state ρ_B^{ath} . This athermality is pronounced when the bath is cold and has a small number of degrees of freedom. The above sequence is a standard implementation of a quantum algorithm with branch selection; no special operation is introduced so far.

Thermodynamic recycling—Apart from the computation, we consider performing a thermodynamic task by the interaction between a target system S and the bath B . Examples include information erasure on S , heat engines, and charging/discharging of a battery. Such tasks generally entail thermodynamic costs such as heat dissipation, as captured by fundamental limits including Lan-

dauer's principle for erasure, thermodynamic uncertainty relations for precision, and the Carnot bound for efficiency. As long as one uses the equilibrium bath $\rho_B^{\text{th}}(T_0)$, these fundamental limits apply, and the corresponding costs cannot be avoided.

We overcome these limits through collaboration with quantum computation. In our thermodynamic recycling, immediately after the reset of a failure branch in the above quantum algorithm, we couple the bath B to the target system S and perform the task operation. Let ρ_S be the initial state of S , and let U_{SB} be the coupling unitary between S and B . The state transitions as

$$\rho_S \otimes \rho_B^{\text{ath}} \xrightarrow{U_{SB}} \rho'_S, \quad \rho'_S = \text{Tr}_B[\rho'_{SB}], \quad \rho'_B = \text{Tr}_S[\rho'_{SB}] \quad (2)$$

where ρ'_S is the post-task state of S and ρ'_B is the bath state. This process defines a completely-positive trace-preserving map on S and can represent a general thermodynamic task. The athermality of the bath can reduce thermodynamic costs below the limits for an equilibrium bath. In particular, deviations of ρ_B^{ath} from the equilibrium distribution and coherences can act as thermodynamic resources. The key point of our method is to couple the bath to the target system before the bath relaxes back to equilibrium. This framework is generic and does not depend on a specific algorithm or thermodynamic task.

One promising application of thermodynamic recycling is in the case of quantum multi-programming [25–29]. The architecture is designed to improve the throughput of quantum computers by running multiple quantum programs simultaneously on a single quantum processor. In such settings, for example, we consider the parallel execution of two quantum programs: one program includes branch selection, while the other program includes quantum error correction. Generally, the error correction protocol requires frequent resets of ancilla qubits and thus reducing heat dissipation is crucial [13, 14, 19]. By applying thermodynamic recycling, we can reduce the heat

dissipation in the error correction protocol by utilizing the athermal bath generated during the reset of failure branches in the other program.

The effectiveness of an athermal bath for performance beyond conventional thermodynamic limits has also been analyzed in reservoir engineering [30–34]. There, the bath is driven out of equilibrium by actively applying a unitary transformation to the bath. However, such an operation itself requires a cost to implement, so it is not advantageous in net thermodynamic terms, rigorously. In contrast, thermodynamic recycling uses an athermal bath that is generated passively during the reset of failure branches, and therefore does not incur an additional cost to manipulate the bath. As a result, when a task performance metric (e.g., the entropy reduction) is fixed, the net thermodynamic cost can be reduced. As an analogy, this is similar to reusing waste heat from power plants or data centers for heating pools. In this sense, our method recycles garbage states produced alongside quantum computation and converts them into resources.

Information erasure— To show that thermodynamic recycling can reduce thermodynamic costs, we analyze information erasure as an example. Let $\Delta S_S = S(\rho_S) - S(\rho'_S)$ be the decrease in the von Neumann entropy of S under the process U_{SB} . Denoting the initial bath state generically as ρ_B , the heat transferred to the bath is $\Delta Q_B = \text{Tr}[H_B(\rho'_B - \rho_B)]$. If the bath is initially in the equilibrium state at temperature T_0 (i.e., $\rho_B = \rho_B^{\text{th}}(T_0)$), Landauer’s principle gives the lower bound $Q_{\text{Landauer}} = k_B T_0 \Delta S_S$ and implies $\Delta Q_B \geq Q_{\text{Landauer}}$ [35–37]. However, for baths in quantum settings that are small and close to absolute zero, the Landauer bound cannot be saturated. A tighter bound $Q_{\text{tight}}(\Delta S_S; T_0)$ under finite-bath constraints has been derived, where Q_{tight} is determined by the bath heat capacity [38] (See Appendix for details). Therefore, our objective is to reduce ΔQ_B below Q_{tight} in the following.

In thermodynamic recycling, the input bath is athermal (i.e., $\rho_B = \rho_B^{\text{ath}}$), and the minimum heat dissipation for the same ΔS_S generally changes from that for a thermal bath. Denoting the corresponding bound by $Q_{\text{ath}}(\Delta S_S; T_0, \rho_B^{\text{ath}})$, one can show

$$Q_{\text{ath}}(\Delta S_S; T_0, \rho_B^{\text{ath}}) = Q_{\text{tight}}(\Delta S_S; T_0) - G(\Delta S_S; T_0, \rho_B^{\text{ath}}). \quad (3)$$

Here, the gain G quantifies the reduction in the minimum dissipation enabled by athermality and is given by

$$\begin{aligned} G(\Delta S_S; T_0, \rho_B^{\text{ath}}) \\ = \Delta E(\rho_B^{\text{ath}}, \rho_B^{\text{th}}(T_0)) - \int_{S(\rho_B^{\text{th}}(T_0))}^{S(\rho_B^{\text{ath}})} \mathcal{T}(s + \Delta S_S) ds. \end{aligned} \quad (4)$$

Here $\mathcal{T}(s)$ denotes the temperature of the Gibbs state of the bath with entropy s , and $\mathcal{T} > 0$. Moreover, $\Delta E(\rho, \sigma) = \text{Tr}[H_B(\rho - \sigma)]$ is the energy difference between ρ and σ . Thus, the gain G is expressed as the

difference between (i) a positive contribution when the athermal state ρ_B^{ath} has higher energy than the equilibrium state $\rho_B^{\text{th}}(T_0)$ and (ii) a negative contribution when the bath entropy increases. If $G > 0$, thermodynamic recycling can, in principle, erase an entropy ΔS_S with heat dissipation smaller than Q_{tight} ; whether this is actually achievable depends on the design of the erasure process U_{SB} and on noise. The derivation of Eq. (3) is given in the Appendix. The equality condition $\Delta Q_B = Q_{\text{ath}}$ holds when the final bath state is a Gibbs state, and the final joint state of the system and bath is uncorrelated.

The branching structure of a quantum algorithm controls the gain. Consider the case with multiple failure branches. For example, in a representative magic-state distillation protocol [4], the process succeeds only when all 14 measurement outcomes are 1, while the remaining $2^{14} - 1$ combinations correspond to failure. Let each failure branch m occur with probability p_m and yield an athermal bath state $\rho_B^{\text{ath}(m)}$ respectively. If the branch information is retained, the average gain is $\bar{G} = \sum_m p_m G(\Delta S_S, \rho_B^{\text{ath}(m)})$. If the branch information is discarded, the gain is evaluated for the mixed athermal bath state $\bar{\rho}_B^{\text{ath}}$ as $G_{\text{mix}} = G(\Delta S_S, \bar{\rho}_B^{\text{ath}})$. We compare these two quantities. Assume that the bath entropies are equal for all m : $S(\rho_B^{\text{ath}(m)}) = S_{\text{failure}}$, which holds when the reset process U_{reset} is identical for each failure branch. Then

$$\begin{aligned} G_{\text{mix}} &= \bar{G} - \int_0^\chi \mathcal{T}(s + \Delta S_S + S_{\text{failure}}) ds \\ &\leq \bar{G}. \end{aligned} \quad (5)$$

Here χ is the Holevo quantity $\chi = S(\bar{\rho}_B^{\text{ath}}) - \sum_m p_m S(\rho_B^{\text{ath}(m)})$, which quantifies our knowledge of the branch index m [39]. Therefore, discarding branch information necessarily reduces the gain.

We further analyze the relationship between the gain and the bath entropy. We fix the bath energy difference $\Delta E > 0$. In this case, whether the gain in Eq. (4) is positive is determined by the bath entropy $S(\rho_B^{\text{ath}})$ appearing in the second term on the right-hand side. Specifically, there exists a threshold S_{max} such that $G > 0$ for $S(\rho_B^{\text{ath}}) < S_{\text{max}}$ and $G < 0$ for $S(\rho_B^{\text{ath}}) > S_{\text{max}}$. Moreover, there is a tradeoff between this threshold and the erasure amount ΔS_S :

$$\frac{\partial S_{\text{max}}}{\partial \Delta S_S} < 0. \quad (6)$$

Here we used the mild assumption $\mathcal{T}(a) > \mathcal{T}(b)$ for $a > b$. Therefore, the smaller the erasure amount ΔS_S , the larger the bath entropy that can be tolerated while still yielding a gain, and vice versa. In particular, for an infinitesimal erasure amount $\Delta S_S \rightarrow +0$, we show that a gain is obtained unless ρ_B^{ath} is a perfect Gibbs state. This universality of the gain is derived in Appendix, including a demonstration on a device.

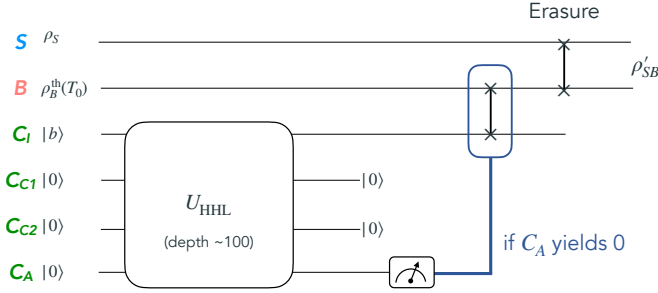


FIG. 2. Circuit sketch of the demonstration protocol. The success/failure of HHL is determined by mid-circuit measurement, and only upon failure, we reset the failure branch by a SWAP with B via feedforward. Before B relaxes, we implement the erasure operation by another SWAP. Full state tomography is performed on S before and after erasure.

Demons—We demonstrate thermodynamic recycling by implementing the HHL algorithm on IBM’s superconducting quantum processor `ibm_kawasaki` (an instance of the “Heron” processor) [20, 40, 41] and performing information erasure. HHL outputs the solution of a linear system $Ax = b$ as a quantum state and selects the success/failure branch by measuring an ancilla. The protocol sketch is shown in Fig. 2. We implement the thermodynamic target system S and the bath B as single qubits. Using a classical feedforward operation [42, 43], only when the HHL algorithm fails, we couple the bath to the failure branch to reset the qubit and prepare an athermal bath. Immediately afterward, we apply an erasure operation to the system and bath and evaluate the heat dissipation associated with information erasure. This experiment tests whether thermodynamic recycling provides a gain on a noisy quantum computer. We note that, in practice, the bath for quantum-computation reset is placed outside the processor; here we reconstruct it inside the processor to track thermodynamic costs.

We use the 2×2 linear-system instance

$$A = \begin{pmatrix} 2 & -1 \\ -1 & 2 \end{pmatrix}, \quad b = \begin{pmatrix} \cos \theta_b \\ \sin \theta_b \end{pmatrix} \quad (7)$$

and sweep θ_b from 0 to $\pi/4$. For the HHL algorithm, we use four qubits as the computational system C : the input/output register C_I (one qubit), the clock register C_C (two qubits), and the rotation ancilla C_A (one qubit). For the HHL implementation, we use simplified constructions from Refs. [44, 45]. In the failure branch, we reset C_I by a classically conditional (i.e., classical feedforward) SWAP between C_I and the bath B .

The initial state of the cold bath B is prepared by natural relaxation of the device. From calibration data, the effective temperature of the bath qubit is estimated to be 43 mK [10, 24, 46]. The mixed state of the target system S is generated by applying an X gate to the initial state $|0\rangle$ with probability p_x . More specifically, we run circuits with and without the X gate and generate the

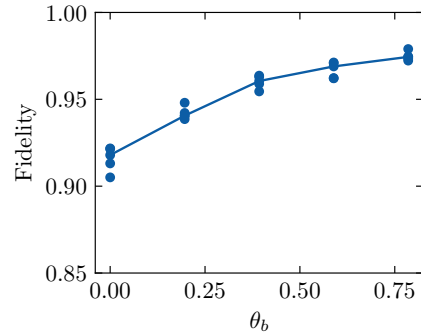


FIG. 3. Fidelity $F(\theta_b)$ of the output state in the success branch of the HHL algorithm. Each point corresponds to a single trial, and the curve connects the medians over multiple trials.

mixed state $\rho_S = p_x |1\rangle\langle 1| + (1 - p_x) |0\rangle\langle 0|$ by classical postprocessing. In this setting, the bound Q_{ath} is, in principle, achieved with equality: $\Delta Q_B = Q_{\text{ath}}$.

We also perform state tomography of S , B , and C_I before and after erasure to estimate the required quantities [47]. To evaluate heat dissipation and the bound Q_{tight} , we need the bath Hamiltonian. We therefore assume the resonance frequency of the bath qubit B to be 5 GHz [46, 48]: the results below do not change qualitatively within the range 3–7 GHz. For expectation-value estimation, we run 8,000 shots for each tomography basis (16,000 shots in total due to the presence/absence of the X gate for preparing S). To estimate fluctuations, we perform five trials for each setting. For comparison, we also perform information erasure using an equilibrium bath: this is implemented in the success branch by swapping S and B without classical feedforward.

We first confirm that the HHL algorithm outputs the desired solution state in the success branch. Specifically, for $\rho_{C_I}^{\text{Suc}}$ obtained by tomography, we compute the fidelity with the ideal solution state $|x(\theta_b)\rangle$ as $F(\theta_b) = \langle x(\theta_b) | \rho_{C_I}^{\text{Suc}} | x(\theta_b) \rangle$, shown in Fig. 3. The fidelity lies in the range 0.92–0.97, indicating that the success branch yields the correct output. The deviation from unity is attributed to noise and errors rather than an implementation mistake.

In the following, we present information-erasure results with the initial mixedness fixed to $p_x = 0.4$. We first evaluate the information erasure for the reference case in which the bath begins in the thermal state at $T_0 = 43$ mK. Figure 4(a) shows the heat dissipation ΔQ_B versus the parameter θ_b . Using the empirical values of ΔS_S and T_0 , we compute Q_{ath} , Q_{tight} , and Q_{Landauer} . In the present setting, $Q_{\text{ath}} = Q_{\text{tight}}$. In the figure, the observed ΔQ_B is greater than these bounds, and the Landauer limit Q_{Landauer} . Moreover, Q_{tight} is much larger than Q_{Landauer} , indicating a significant finite-size and low-temperature effect of the bath relative to the conventional Landauer limit.

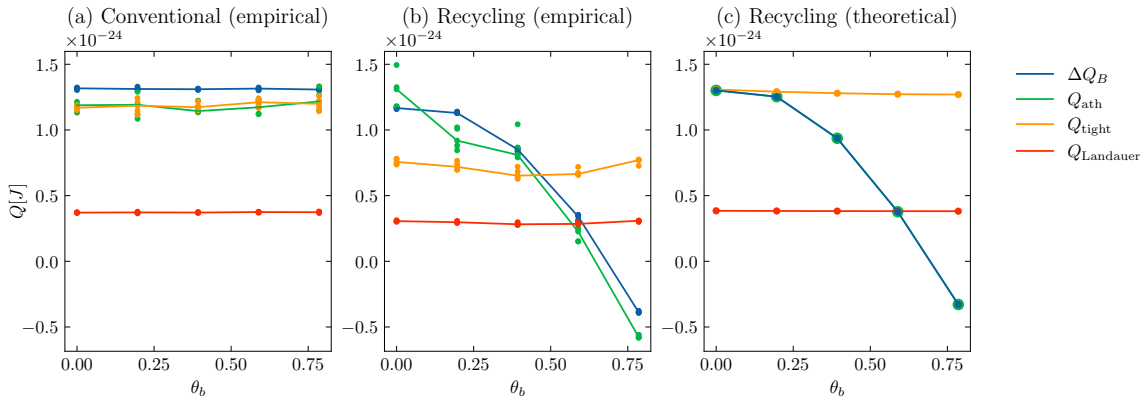


FIG. 4. Information-erasure results on ibm_kawasaki. (a) Erasure using an equilibrium bath. (b) Experimental results for erasure using thermodynamic recycling. (c) Theoretical prediction for erasure using thermodynamic recycling. The horizontal axis is the parameter θ_b , and the vertical axis is the heat dissipation ΔQ_B and the theoretical bounds Q_{ath} , Q_{tight} , and Q_{Landauer} . Each point corresponds to a single trial, and the curve connects the medians over multiple trials.

Our main result, information erasure using thermodynamic recycling, is shown in Fig. 4(b). Here we use the athermal bath ρ_B^{ath} originating from the failure branch. Note that the bounds Q_{ath} , Q_{tight} , and Q_{Landauer} differ from those in Fig. 4(a) because they are computed from the empirical ΔS_S , which differs largely between the two cases. Since Q_{tight} and Q_{Landauer} are computed from the intrinsic temperature T_0 , they represent the lower bounds for erasing ΔS_S using the thermal bath. The lines in the figure connect the medians over multiple trials. The data show a regime where the empirical heat dissipation ΔQ_B is below the equilibrium bound Q_{tight} ; for larger θ_b , ΔQ_B can also fall below the Landauer limit Q_{Landauer} . These results indicate that, for erasing a given ΔS_S , the minimum heat dissipation is reduced to a level that cannot be achieved with an equilibrium bath. Equivalently, thermodynamic recycling reduces the *net* heat dissipation required to erase ΔS_S compared to the case where we perform HHL and erasure separately. This is the main achievement of this work. We also find that, for most θ_b , ΔQ_B is above the bound Q_{ath} , consistent with theory; the bound violation at $\theta_b = 0$ is attributed to device errors and estimation errors of the von Neumann entropy

Next, we compare the empirical results with the theoretical prediction. Figure 4(c) shows the theoretical values for thermodynamic recycling assuming the bath at $T_0 = 43$ mK. Here, the heat dissipation ΔQ_B coincides with its lower bound Q_{ath} , indicating that the present experimental setting satisfies the equality conditions. The figure shows that, for all θ_b , ΔQ_B lies below the equilibrium-bath limit Q_{tight} . For larger θ_b , ΔQ_B can also lie below the Landauer limit Q_{Landauer} . These theoretical predictions are qualitatively consistent with the experimental results. In the experiment, however, the bath athermality is degraded by noise and feedforward latency, which likely reduces the gain relative to the theory. This degradation is a plausible cause of $\Delta Q_B > Q_{\text{tight}}$ in

the small- θ_b regime. The Appendix includes an analysis of the time required for classical feedforward. It indicates that the HHL part (whose depth is about 100) takes 4.0 μs , whereas feedforward operation+SWAP takes 3.3 μs (See Appendix). This latency is non-negligible compared to the qubit relaxation time $T_1 = 397$ μs of the bath qubit. Our results thus demonstrate the feasibility of thermodynamic recycling under such device constraints of current quantum computers.

Concluding remarks—We proposed a framework that exploits failure branches, previously discarded in quantum computing, as a resource and demonstrated it on hardware. The significance of the demonstration is not the task itself, but that we executed, on a single device, (i) running an algorithm with postselection, (ii) conditional processing of the failure branch (classical feedforward operation), (iii) coupling before bath relaxation, and (iv) measuring heat dissipation and entropy reduction. In our approach, thermodynamic resource generation and utilization are subject to the same constraints as algorithm execution (gate errors, latency, and initial mixedness), and the feasibility of resource conversion is inseparable from hardware conditions, highlighted in our demonstrations. The applicability of thermodynamic recycling is not specific to a particular algorithm or thermodynamic task. Therefore, a promising direction for future work is to explore a broad class of computational subroutines and thermodynamic tasks to gain insights into the design of efficient quantum computers from a thermodynamic perspective.

Acknowledgments—We acknowledge the use of IBM Quantum services for this work. The views expressed are those of the authors, and do not reflect the official policy or position of IBM or the IBM Quantum team.

Appendix

Derivation of the lower bound Q_{ath}

We derive the lower bound Q_{ath} in Eq. (3). As a starting point, we clarify the tight bound Q_{tight} in the main text. Let the initial bath state be the thermal state at temperature T_0 : $\rho_B = \rho_B^{\text{th}}(T_0)$. The tight bound $Q_{\text{tight}}(\Delta S_S; T_0)$ for erasing an entropy ΔS_S is given by [38]:

$$Q_{\text{tight}}(-\Delta S_S; T_0) = \mathcal{Q}(\mathcal{S}^{-1}(-\Delta S_S; T_0); T_0), \quad (8)$$

where the functions \mathcal{S} and \mathcal{Q} are defined as

$$\mathcal{S}(T; T_0) = \int_{T_0}^T \frac{\mathcal{C}_B(\tau)}{k_B \tau} d\tau, \quad \mathcal{Q}(T; T_0) = \int_{T_0}^T \mathcal{C}_B(\tau) d\tau. \quad (9)$$

Here, $\mathcal{C}_B(T)$ is the heat capacity of the bath at temperature T . The equality condition $\Delta Q_B = Q_{\text{tight}}$ holds when the final bath state is a Gibbs state, and the final joint state of the system and bath is uncorrelated.

Next, we derive the bound Q_{ath} for an athermal bath ρ_B^{ath} . Our derivation is based on the positivity of mutual information and the MaxEnt principle, based on Ref. [38]. The mutual information between S and B after the erasure process is $I_{SB} = S(\rho'_S) + S(\rho'_B) - S(\rho'_{SB}) \geq 0$. Using the fact that the initial entropy is given by $S(\rho_S) + S(\rho_B^{\text{ath}})$ and that the von Neumann entropy is invariant under unitary evolution, we have $\Delta S_B \geq \Delta S_S$, where $\Delta S_B = S(\rho'_B) - S(\rho_B^{\text{ath}})$ is the change in the bath entropy. Therefore, to erase an entropy ΔS_S from the system, the bath entropy must increase by at least ΔS_S .

We consider the case where the athermal bath ρ_B^{ath} has the same entropy as the thermal state at temperature T_0 : $S(\rho_B^{\text{ath}}) = S(\rho_B^{\text{th}}(T_0))$. Then, among the states with entropy at least $S(\rho_B^{\text{th}}(T_0)) + \Delta S_S$, the Gibbs state at temperature $\mathcal{S}^{-1}(\Delta S_S; T_0)$ minimizes the energy due to the MaxEnt principle. In this case, we have

$$\Delta Q_B \geq Q_{\text{tight}}(\Delta S_S; T_0) - \Delta E(\rho_B^{\text{ath}}, \rho_B^{\text{th}}(T_0)), \quad (10)$$

where $\Delta E(\rho_B^{\text{ath}}, \rho_B^{\text{th}}(T_0))$ is the energy difference between ρ_B^{ath} and $\rho_B^{\text{th}}(T_0)$.

Now, we consider the general case where $S(\rho_B^{\text{ath}})$ can differ from $S(\rho_B^{\text{th}}(T_0))$. Let the difference be $r = S(\rho_B^{\text{ath}}) - S(\rho_B^{\text{th}}(T_0))$. When the bath entropy increases ΔS_S , the final bath entropy becomes

$$S(\rho'_B) = S(\rho_B^{\text{ath}}) + \Delta S_S = S(\rho_B^{\text{th}}(T_0)) + \Delta S_S + r. \quad (11)$$

Therefore, the bath requires additional energy cost due to the extra entropy r given by

$$\int_0^r \mathcal{T}(s + \Delta S_S + S(\rho_B^{\text{th}}(T_0))) ds = \int_{S(\rho_B^{\text{th}}(T_0))}^{S(\rho_B^{\text{ath}})} \mathcal{T}(s + \Delta S_S) ds, \quad (12)$$

where we used the relation $\mathcal{T}(s) = \frac{\partial E}{\partial S}|_{S=s}$. Combining this with Eq. (10), we obtain the lower bound for an athermal bath:

$$\begin{aligned} \Delta Q_B &\geq Q_{\text{tight}}(\Delta S_S; T_0) - \Delta E(\rho_B^{\text{ath}}, \rho_B^{\text{th}}(T_0)) \\ &\quad + \int_{S(\rho_B^{\text{th}}(T_0))}^{S(\rho_B^{\text{ath}})} \mathcal{T}(s + \Delta S_S) ds. \end{aligned} \quad (13)$$

This is the desired result in Eq. (3).

Analysis of the gain depending on the branch information

The gain depends on the bath entropy: intuitively, the lower the bath entropy, the larger the gain. Here, we analyze how branch information affects the gain when multiple failure branches are present. Let each failure branch m occur with probability p_m and yield an athermal bath state $\rho_B^{\text{ath}(m)}$ respectively. As in the main text, we assume that the bath entropies are equal for all m : $S(\rho_B^{\text{ath}(m)}) = S_{\text{failure}}$. The gain for each branch is given by $G^{(m)} = G(\Delta S_S; T_0, \rho_B^{\text{ath}(m)})$. The average gain is given by

$$\begin{aligned} \bar{G} &= \sum_{m=1}^M p_m G^{(m)} \\ &= \sum_{m=1}^M p_m \Delta E(\rho_B^{\text{ath}(m)}, \rho_B^{\text{th}}(T_0)) - \int_{S(\rho_B^{\text{th}}(T_0))}^{S_{\text{failure}}} f(s - \Delta S_S) ds. \end{aligned} \quad (14)$$

As the energy difference is linear in the state, we have

$$\bar{G} = \Delta E(\bar{\rho}_B^{\text{ath}}, \rho_B^{\text{th}}(T_0)) - \int_{S(\rho_B^{\text{th}}(T_0))}^{S_{\text{failure}}} f(s - \Delta S_S) ds, \quad (15)$$

where $\bar{\rho}_B^{\text{ath}} = \sum_{m=1}^M p_m \rho_B^{\text{ath}(m)}$ is the average bath state.

On the other hand, if we discard the branch information before erasure, the bath state becomes the mixture $\bar{\rho}_B^{\text{ath}}$. Due to the concavity of the von Neumann entropy, the bath entropy increases as

$$S(\bar{\rho}_B^{\text{ath}}) = S\left(\sum_{m=1}^M p_m \rho_B^{\text{ath}(m)}\right) \geq \sum_{m=1}^M p_m S(\rho_B^{\text{ath}(m)}) = S_{\text{failure}}. \quad (16)$$

Here, the increase is quantified by the Holevo quantity

$$\chi = S(\bar{\rho}_B^{\text{ath}}) - S_{\text{failure}} > 0, \quad (17)$$

which quantifies our knowledge of the branch index m [39]. Therefore, the bath entropy is now $S(\bar{\rho}_B^{\text{ath}}) =$

$S_{\text{failure}} + \chi$. Using the quantity χ , the gain for the mixed bath state is given by

$$\begin{aligned} G_{\text{mix}} &= \Delta E(\bar{\rho}_B^{\text{ath}}, \rho_B^{\text{th}}(T_0)) - \int_{S(\rho_B^{\text{th}}(T_0))}^{S(\bar{\rho}_B^{\text{ath}})} \mathcal{T}(s + \Delta S_S) ds \\ &= \Delta E(\bar{\rho}_B^{\text{ath}}, \rho_B^{\text{th}}(T_0)) - \int_{S(\rho_B^{\text{th}}(T_0))}^{S_{\text{failure}} + \chi} \mathcal{T}(s + \Delta S_S) ds \\ &= \bar{G} - \int_{S_{\text{failure}}}^{S_{\text{failure}} + \chi} \mathcal{T}(s + \Delta S_S) ds \\ &= \bar{G} - \int_0^{\chi} \mathcal{T}(s + \Delta S_S + S_{\text{failure}}) ds. \end{aligned} \quad (18)$$

As $\mathcal{T} > 0$ and $\chi > 0$, we have $G_{\text{mix}} \leq \bar{G}$. Therefore, the more we know about the branch index m , the greater the gain we can obtain, and vice versa.

Tradeoff between the erasure amount and the maximum tolerable bath entropy: theoretical results and demonstration

As we have described in the main text, there exists a threshold S_{max} for the bath entropy such that a gain is obtained for $S(\rho_B^{\text{ath}}) < S_{\text{max}}$: otherwise, no gain is obtained. We detail this theory here. Fix the bath energy difference $\Delta E > 0$ and denote the athermal bath energy by $E^{\text{ath}} = \text{Tr}[H_B \rho_B^{\text{ath}}]$. Now, we consider the limit of infinitesimal erasure amount $\Delta S_S \rightarrow +0$. In this limit, we can show the following tradeoff relation:

$$\frac{S_{E^{\text{ath}}} - S_{\text{max}}}{\Delta S_S} \geq 1 - \frac{T_0}{T_{E^{\text{ath}}}}, \quad (19)$$

where $S_{E^{\text{ath}}}$ is the entropy of the Gibbs state with energy E^{ath} and $T_{E^{\text{ath}}}$ is its temperature. By the MaxEnt principle, $S_{E^{\text{ath}}} \geq S_{\text{max}}$. For $\Delta E > 0$, $T_{E^{\text{ath}}} > T_0$ holds in typical systems, so the right-hand side is positive. Therefore, Eq. (19) captures the universality of the gain. That is, for any ρ_B^{ath} , unless it is a perfect equilibrium state, $S_{E^{\text{ath}}} > S_{\text{max}}$ holds, and for sufficiently small ΔS_S a gain is obtained. We postpone the derivation of these results to the end of this subsection.

We consider the practical implications of Eq. (19). In the demonstration in the main text, we observed that thermodynamic recycling yields a gain for certain θ_b but not for others. In particular, at $\theta_b = 0$, no gain was observed. Now we vary the amount of erasure ΔS_S to investigate whether a gain can be obtained even at $\theta_b = 0$ following the above prediction. When no gain is obtained, i.e., when $\Delta Q_B > Q_{\text{tight}}$, the bath entropy of the pre-erasure state ρ_B^{ath} is expected to exceed the maximum tolerable value S_{max} . The above theory implies, through Eqs. (6) and (19), that the smaller the erasure amount ΔS_S , the larger the margin for obtaining a gain.

To investigate how the gain depends on ΔS_S , we sweep the initial mixedness p_x of the target system. A

smaller p_x yields a smaller initial entropy $S(\rho_S)$ and thus a smaller erasure amount ΔS_S . Figure 5(a) shows the experimental results for thermodynamic recycling at $\theta_b = 0$. The horizontal axis is p_x , and the vertical axis is the heat dissipation ΔQ_B and the theoretical lower bounds. We plot only the erasure-success regime, i.e., $\Delta S_S > 0$. The value at $p_x = 0.4$ corresponds to $\theta_b = 0$ in Fig. 4(b). As p_x decreases, ΔQ_B decreases, and it intersects the equilibrium-bath bound Q_{tight} around $p_x \sim 0.03$. To make this trend clearer, Fig. 5(b) shows the dissipation ratio $(\Delta Q_B - Q_{\text{tight}})/Q_{\text{tight}}$. This ratio is negative when the dissipation lies below the bound. The figure plots the results for all θ_b . For all θ_b , $\Delta Q_B < Q_{\text{tight}}$ holds for sufficiently small p_x . Note that, in this regime, the erasure amount ΔS_S is small. Therefore, the experimental results are consistent with the prediction of Eq. (19): for sufficiently small erasure amounts, thermodynamic recycling yields a gain.

We now derive Eqs. (6) and (19). By solving the equation $G(\Delta S_S; T_0, \rho_B^{\text{ath}}) = 0$ for $S(\rho_B^{\text{ath}})$, we obtain the threshold S_{max} as:

$$\begin{aligned} S_{\text{max}}(E_h) \\ = \mathcal{S}(\mathcal{Q}^{-1}(E^{\text{ath}} - E_B[\rho_B^{\text{th}}(T_0)]; T'); T') + S(\rho_B^{\text{th}}(T_0)), \end{aligned} \quad (20)$$

where

$$T' = \mathcal{S}^{-1}(-\Delta S_S; T_0). \quad (21)$$

To calculate the derivative of S_{max} with respect to ΔS_S , we use the implicit function theorem. We have

$$\frac{\partial S_{\text{max}}}{\partial \Delta S_S} = \frac{\mathcal{T}(S(\rho_B^{\text{th}}(T_0) - \Delta S_S))}{\mathcal{T}(S_{\text{max}} - \Delta S_S)} - 1. \quad (22)$$

Under the weak assumption of $\mathcal{T}(a) > \mathcal{T}(b)$ for $a > b$, we have $\frac{\partial S_{\text{max}}}{\partial \Delta S_S} \leq 0$, which is Eq. (6). Then, we obtain Eq. (19) by taking the limit $\Delta S_S \rightarrow +0$ in Eq. (22) and using the Taylor expansion.

Analysis of the feedforward latency

In our demonstration, we analyze the time required for the HHL algorithm and the classical feedforward operation. From the official calibration data of `ibm_kawasaki` [20], the gate time for a single-qubit gate is 32 ns, and that for a two-qubit gate is 68 ns. However, the time required for classical feedforward operations is not provided in the calibration data. Therefore, we estimate it by using the method called “gate-time amplification”, which was proposed in Ref. [49]. This method estimates the execution time of a target gate (or operation) from the total execution time of a job submitted to the quantum processor. Although the job time is measured coarsely (with a resolution of 1 s), this method can estimate the gate time

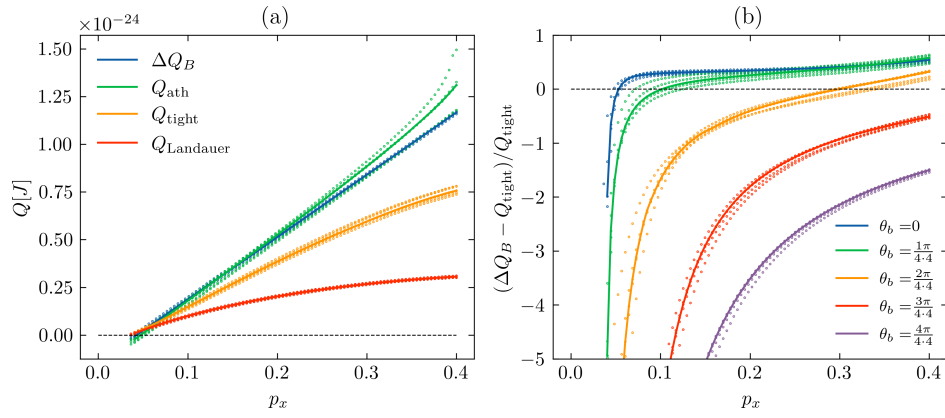


FIG. 5. Dependence of heat dissipation ΔQ_B on the initial mixedness p_x of the target system. (a) Empirical heat dissipation ΔQ_B and the theoretical bounds Q_{ath} , Q_{tight} , and Q_{Landauer} for $\theta_b = 0$. (b) Results for the dissipation ratio $(\Delta Q_B - Q_{\text{tight}})/Q_{\text{tight}}$ for all θ_b . The list of θ_b is the same as in Fig. 4. In both (a) and (b), we plot only the regime where $\Delta S_S > 0$. Each point corresponds to a single trial, and the curves connect the medians over multiple trials.

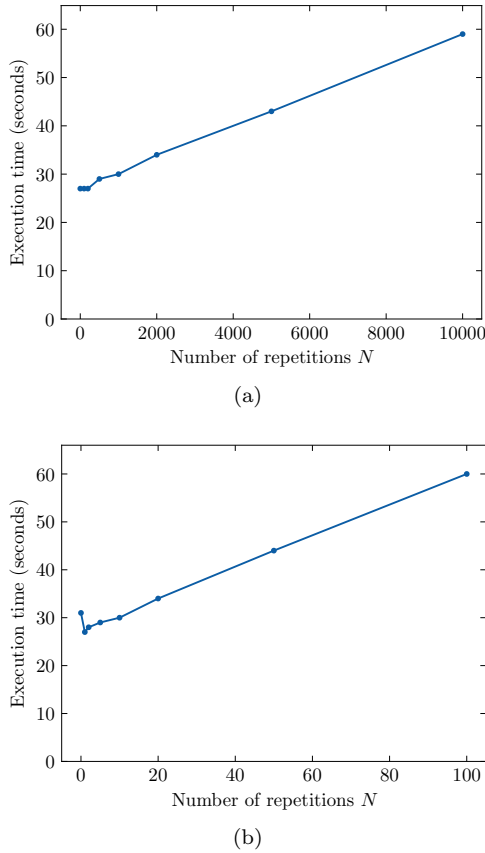


FIG. 6. Execution time of the circuits composed of (a) X gates and (b) classical feedforward operations.

to within a few nanoseconds by amplifying it. Moreover, this method can avoid the various overheads involved in job execution, such as qubit reset time and classical post-processing time, which are unknown to users.

In the method, we vary the number of target gates N

in the circuit and measure the total execution time of the job. By fitting the data with a linear function, we can estimate the execution time of a single target gate as the slope of the fitted line. To amplify the gate time, we repeat the measurement (shots) $N_{\text{shots}} = 10,000$ times for the same circuit and repeat it $N_{\text{circ}} = 10$ times in a single job.

We first estimate the execution time of a circuit composed of only X gates as a reference. Figure 6(a) shows the total execution time T_{total} versus the number of X gates. We see that the data are well described by a linear function for sufficiently large repetitions ($N > 2,000$). From the fitting to the regime, we estimate the execution time of a X gate to be 31.3 ns, consistent with the calibration data (32 ns). Next, we estimate the execution time of a circuit composed of classical feedforward operations, which include measurements and conditional SWAP gates on the bath B and the computational qubit C_I . Figure 6(b) shows the total execution time versus the number of classical feedforward operations. From the fitting for the regime $N > 20$, we estimate the execution time of a single classical feedforward operation as 3.3 μ s.

* ishida@biom.t.u-tokyo.ac.jp

† hasegawa@biom.t.u-tokyo.ac.jp

- [1] A. W. Harrow, A. Hassidim, and S. Lloyd, Quantum algorithm for linear systems of equations, *Phys. Rev. Lett.* **103**, 150502 (2009).
- [2] A. Gilyén, Y. Su, G. H. Low, and N. Wiebe, Quantum singular value transformation and beyond: exponential improvements for quantum matrix arithmetics, in *Proceedings of the 51st Annual ACM SIGACT Symposium on Theory of Computing* (ACM, New York, NY, USA, 2019).
- [3] J. M. Martyn, Z. M. Rossi, A. K. Tan, and I. L. Chuang,

Grand unification of quantum algorithms, *PRX Quantum* **2**, 040203 (2021).

[4] S. Bravyi and A. Kitaev, Universal quantum computation with ideal Clifford gates and noisy ancillas, *Phys. Rev. A* **71**, 022316 (2005).

[5] S. Bravyi and J. Haah, Magic-state distillation with low overhead, *Phys. Rev. A* **86**, 052329 (2012).

[6] M. Howard and E. Campbell, Application of a resource theory for magic states to fault-tolerant quantum computing, *Phys. Rev. Lett.* **118**, 090501 (2017).

[7] L. K. Grover, A fast quantum mechanical algorithm for database search, in *Proceedings of the twenty-eighth annual ACM symposium on Theory of computing - STOC '96* (ACM Press, New York, New York, USA, 1996) p. 212.

[8] D. W. Berry, A. M. Childs, R. Cleve, R. Kothari, and R. D. Somma, Exponential improvement in precision for simulating sparse Hamiltonians, in *Proceedings of the forty-sixth annual ACM symposium on Theory of computing* (ACM, New York, NY, USA, 2014).

[9] C. Gidney, N. Shutty, and C. Jones, Magic state cultivation: growing T states as cheap as CNOT gates, [arXiv:2409.17595](https://arxiv.org/abs/2409.17595) (2024).

[10] L. Buffoni, S. Gherardini, E. Zambrini Cruzeiro, and Y. Omar, Third Law of Thermodynamics and the Scaling of Quantum Computers, *Phys. Rev. Lett.* **129**, 150602 (2022).

[11] M. A. Aamir, P. Jamet Suria, J. A. Marín Guzmán, C. Castillo-Moreno, J. M. Epstein, N. Yunger Halpern, and S. Gasparinetti, Thermally driven quantum refrigerator autonomously resets a superconducting qubit, *Nat. Phys.* **21**, 318 (2025).

[12] M. S. Blok and G. T. Landi, Quantum thermodynamics for quantum computing, *Nat. Phys.* **21**, 187 (2025).

[13] G. T. Landi, A. L. Fonseca de Oliveira, and E. Buksman, Thermodynamic analysis of quantum error-correcting engines, *Phys. Rev. A* **101**, 042106 (2020).

[14] A. Danageozian, M. M. Wilde, and F. Buscemi, Thermodynamic Constraints on Quantum Information Gain and Error Correction: A Triple Trade-Off, *PRX Quantum* **3**, 020318 (2022).

[15] S. Campbell, I. D'Amico, M. A. Ciampini, J. Anders, N. Ares, S. Artini, A. Auffèves, L. B. Oftelie, L. P. Bettmann, M. V. S. Bonança, T. Busch, M. Campisi, M. F. Cavalcante, L. A. Correa, E. Cuestas, C. B. Dag, S. Dago, S. Deffner, A. del Campo, A. Deutschmann-Olek, S. Donadi, E. Doucet, C. Elouard, K. Ensslin, P. Erker, N. Fabbri, F. Fedele, G. Fiura, T. Fogarty, J. A. Folk, G. Guarneri, A. S. Hegde, S. Hernández-Gómez, C.-K. Hu, F. Iemini, B. Karimi, N. Kiesel, G. Landi, A. Lasek, S. Lemziakov, G. Lo Monaco, E. Lutz, D. Lvov, O. Maillet, M. Mehboudi, T. M. Mendonça, H. J. D. Miller, A. K. Mitchell, M. Mitchison, V. Mukherjee, M. Paternostro, J. P. Pekola, M. Perarnau-Llobet, U. G. Poschinger, A. Rolandi, D. Rosa, R. Sánchez, A. C. Santos, R. S. Sarthour, E. Sela, A. Solfanelli, A. M. Souza, J. Splettstoesser, D. Tan, L. Tesser, T. Van Vu, A. Widera, N. Yunger Halpern, and K. Zawadzki, Roadmap on Quantum Thermodynamics, *Quantum Sci. Technol.* [10.1088/2058-9565/ae1e27](https://doi.org/10.1088/2058-9565/ae1e27) (2025).

[16] T. Śmierzchalski, Z. Mzaouali, S. Deffner, and B. Garidas, Efficiency optimization in quantum computing: balancing thermodynamics and computational performance, *Sci. Rep.* **14**, 4555 (2024).

[17] S. Simbierowicz, M. Borrelli, V. Monarkha, V. Nuutinen, and R. E. Lake, Inherent thermal-noise problem in addressing qubits, *PRX Quantum* **5**, 030302 (2024).

[18] S. Krinner, S. Storz, P. Kurpiers, P. Magnard, J. Heinssoo, R. Keller, J. Lütolf, C. Eichler, and A. Wallraff, Engineering cryogenic setups for 100-qubit scale superconducting circuit systems, *EPJ Quantum Technol.* **6**, 2 (2019).

[19] M. Bilokur, S. Gopalakrishnan, and S. Majid, Thermodynamic limitations on fault-tolerant quantum computing, [arXiv:2411.12805](https://arxiv.org/abs/2411.12805) (2024).

[20] IBM, IBM Quantum, <https://quantum.ibm.com/>, accessed: 2025-12-1.

[21] D. Ristè, C. C. Bultink, K. W. Lehnert, and L. DiCarlo, Feedback control of a solid-state qubit using high-fidelity projective measurement, *Phys. Rev. Lett.* **109**, 240502 (2012).

[22] P. Krantz, M. Kjaergaard, F. Yan, T. P. Orlando, S. Gustavsson, and W. D. Oliver, A quantum engineer's guide to superconducting qubits, *Appl. Phys. Rev.* **6**, 021318 (2019).

[23] Y. Zhou, Z. Zhang, Z. Yin, S. Huai, X. Gu, X. Xu, J. Allcock, F. Liu, G. Xi, Q. Yu, H. Zhang, M. Zhang, H. Li, X. Song, Z. Wang, D. Zheng, S. An, Y. Zheng, and S. Zhang, Rapid and unconditional parametric reset protocol for tunable superconducting qubits, *Nat. Commun.* **12**, 5924 (2021).

[24] L. Bassman Oftelie, A. De Pasquale, and M. Campisi, Dynamic cooling on contemporary quantum computers, *PRX Quantum* **5**, 030309 (2024).

[25] P. Das, S. S. Tannu, P. J. Nair, and M. Qureshi, A Case for Multi-Programming Quantum Computers, in *Proceedings of the 52nd Annual IEEE/ACM International Symposium on Microarchitecture* (ACM, New York, NY, USA, 2019).

[26] X. Dou and L. Liu, A new qubits mapping mechanism for multi-programming quantum computing, in *Proceedings of the ACM International Conference on Parallel Architectures and Compilation Techniques* (ACM, New York, NY, USA, 2020).

[27] S. Niu and A. Todri-Sanial, Enabling multi-programming mechanism for quantum computing in the NISQ era, *Quantum* **7**, 925 (2023).

[28] S. Niu and A. Todri-Sanial, Multi-programming cross platform benchmarking for quantum computing hardware, [arXiv:2206.03144](https://arxiv.org/abs/2206.03144) (2022).

[29] Accelerate quantum programs with parallel execution! Now available via the quantum computer cloud service of The University of Osaka (in Japanese), https://resou.osaka-u.ac.jp/ja/research/2024/20241015_2, accessed: 2026-1-12.

[30] A. Mari and J. Eisert, Cooling by heating: very hot thermal light can significantly cool quantum systems, *Phys. Rev. Lett.* **108**, 120602 (2012).

[31] J. Roßnagel, O. Abah, F. Schmidt-Kaler, K. Singer, and E. Lutz, Nanoscale heat engine beyond the Carnot limit, *Phys. Rev. Lett.* **112**, 030602 (2014).

[32] M. Konopik, A. Friedenberger, N. Kiesel, and E. Lutz, Nonequilibrium information erasure below $kT\ln 2$, *Europhys. Lett.* **131**, 60004 (2020).

[33] Q. Zhang, Z.-X. Man, Y.-J. Zhang, W.-B. Yan, and Y.-J. Xia, Quantum thermodynamics in nonequilibrium reser-

voirs: Landauer-like bound and its implications, *Phys. Rev. A* **107**, 042202 (2023).

[34] S. Campbell, G. Guarneri, M. Paternostro, and B. Vacchini, Nonequilibrium quantum bounds to Landauer's principle: Tightness and effectiveness, *Phys. Rev. A* **96**, 042109 (2017).

[35] R. Landauer, Irreversibility and heat generation in the computing process, *IBM Journal of Research and Development* **5**, 183 (1961).

[36] M. Esposito, K. Lindenberg, and C. Van den Broeck, Entropy production as correlation between system and reservoir, *New J. Phys.* **12**, 013013 (2010).

[37] D. Reeb and M. M. Wolf, An improved Landauer principle with finite-size corrections, *New J. Phys.* **16**, 103011 (2014).

[38] A. M. Timpanaro, J. P. Santos, and G. T. Landi, Landauer's principle at zero temperature, *Phys. Rev. Lett.* **124**, 240601 (2020).

[39] M. A. Nielsen and I. L. Chuang, *Quantum Computation and Quantum Information: 10th Anniversary Edition* (Cambridge University Press, 2010).

[40] IBM, IBM debuts next-generation quantum processor & IBM Quantum System Two, extends roadmap to advance era of quantum utility, <https://newsroom.ibm.com/2023-12-04-IBM-Debuts-Next-Generation-Quantum-Processor-IBM-Quantum-System-Two,-Extends-Roadmap-to-Advance-Era-of-Quantum-Utility>, accessed: 2015-12-1.

[41] D. C. McKay, I. Hincks, E. J. Pritchett, M. Carroll, L. C. G. Govia, and S. T. Merkel, Benchmarking quantum processor performance at scale, arXiv:2311.05933 (2023).

[42] E. Bäumer, V. Tripathi, D. S. Wang, P. Rall, E. H. Chen, S. Majumder, A. Seif, and Z. K. Minev, Efficient long-range entanglement using dynamic circuits, *PRX Quantum* **5**, 030339 (2024).

[43] E. Bäumer, V. Tripathi, A. Seif, D. Lidar, and D. S. Wang, Quantum Fourier transform using dynamic circuits, *Phys. Rev. Lett.* **133**, 150602 (2024).

[44] Y. Zheng, C. Song, M.-C. Chen, B. Xia, W. Liu, Q. Guo, L. Zhang, D. Xu, H. Deng, K. Huang, Y. Wu, Z. Yan, D. Zheng, L. Lu, J.-W. Pan, H. Wang, C.-Y. Lu, and X. Zhu, Solving systems of linear equations with a superconducting quantum processor, *Phys. Rev. Lett.* **118**, 210504 (2017).

[45] Y. Lee, J. Joo, and S. Lee, Hybrid quantum linear equation algorithm and its experimental test on IBM Quantum Experience, *Sci. Rep.* **9**, 4778 (2019).

[46] A. Solfanelli, A. Santini, and M. Campisi, Experimental verification of fluctuation relations with a quantum computer, *PRX Quantum* **2**, 030353 (2021).

[47] J. A. Smolin, J. M. Gambetta, and G. Smith, Efficient method for computing the maximum-likelihood quantum state from measurements with additive Gaussian noise, *Phys. Rev. Lett.* **108**, 070502 (2012).

[48] N. Ishida and Y. Hasegawa, Quantum-computer-based verification of quantum thermodynamic uncertainty relation, *Phys. Rev. E* **112**, 034124 (2025).

[49] N. Ishida and Y. Hasegawa, Energy inference of black-box quantum computers using quantum speed limit, arXiv:2512.15472 (2025).